



Vrije Universiteit Brussel

FACULTEIT GENEESKUNDE EN FARMACIE i.s.m  
FACULTEIT LICHAAMELIJKE OPVOEDING EN KINESITHERAPIE  
Master na Master in Manuele Therapie

# Detection of Kinematic Changes Induced by Sequential Lateral Collateral Ankle Ligament Section: A 4DCT Study.

Detectie van Kinematische Veranderingen na Opeenvolgende  
Sectie van de Laterale Collaterale Ligamenten van de Enkel:  
Een 4DCT Studie.

Masterproef aangeboden tot het behalen van het diploma van  
Master na Master in de Manuele Therapie door:

**Jildert Apperloo**

Academiejaar 2017 – 2018

Promotor: Prof. Dr. Erik Cattrysse

Co-promotor: Luca Buzzatti en Benyameen Keelson











Vrije Universiteit Brussel

FACULTEIT GENEESKUNDE EN FARMACIE i.s.m  
FACULTEIT LICHAAMELIJKE OPVOEDING EN KINESITHERAPIE  
Master na Master in Manuele Therapie

# Detection of Kinematic Changes Induced by Sequential Lateral Collateral Ankle Ligament Section: A 4DCT Study.

Detectie van Kinematische Veranderingen na Opeenvolgende  
Sectie van de Laterale Collaterale Ligamenten van de Enkel:  
Een 4DCT Studie.

Masterproef aangeboden tot het behalen van het diploma van  
Master na Master in de Manuele Therapie door:

**Jildert Apperloo**

Academiejaar 2017 – 2018

Promotor: Prof. Dr. Erik Cattrysse

Co-promotor: Luca Buzzatti en Benyameen Keelson





Aantal woorden artikel: 3015 (Abstract: 242)

Meegewerkt aan dataverzameling: ja

Statistische analyses zelf uitgevoerd: ja

GEZIEN en GOEDGEKEURD

.....

Promotor(en) van de masterproef,

.....

## **Foreword**

This research project would not have been possible without the help of various people. Therefore, I would like to thank a few people. First, I would like to thank my promoter Prof. Dr. Erik Cattrysse for making it possible for me to graduate with this research. Secondly, with equal contribution, I would like to thank Luca Buzzatti and Benyameen Keelson for working most of the time with me to complete this research. Also, much appreciation goes out to the research group for providing feedback. I must also thank the academic staff from the VUB and the people working at the department of radiology of the UZ Brussels for providing all the necessary things to complete this study. Last, I would like to thank my family and friends for supporting me throughout the journey to become a Master in Manual Therapy. I hope you will enjoy reading this manuscript. Best regards, Jildert Apperloo

## **Tabel of contents**

<b>Abstract</b> .....	9
<b>1. Introduction</b> .....	10
<b>2. Materials and Methods</b> .....	11
<b>2.1. Specimen</b> .....	11
<b>2.2. Experimental setup</b> .....	11
<b>2.3. Imaging processing</b> .....	12
<b>2.4. Kinematic analysis</b> .....	14
<b>2.5. Data analysis</b> .....	14
<b>3. Results</b> .....	15
<b>3.1. Repeatability</b> .....	15
<b>3.2. Differences between scenarios</b> .....	17
<b>4. Discussion</b> .....	21
<b>5. Conclusion</b> .....	23
<b>References</b> .....	24

## **Abstract**

**Objectives:** Exploring the feasibility of dynamic computed tomography to detect kinematic changes, induced by sequential sectioning of the lateral collateral ligaments of the ankle, during full motion sequence of the talocrural and subtalar joint.

**Materials and Methods:** A custom-made device was used to induce cyclic controlled ankle inversion movement in one fresh frozen cadaver leg. A 256-slice CT scanner was used to investigate four different scenarios. First, Scenario 1 with all ligaments intact was investigated followed by sequential section of the anterior talo-fibular ligament (Scenario 2), the calcaneo-fibular ligament (Scenario 3) and posterior talo-fibular ligament (Scenario 4). Off-line image processing based on semi-automatic segmentation and bone rigid registration was performed. Motion parameters such as translation, rotational angles and orientation and position of the axis of rotation were calculated from registration outputs. Differences between scenarios were calculated for the talocrural and subtalar joint.

**Results:** The setup showed to be reliable with differences between repetitions below  $1^\circ$  for rotation angles and below 0.7mm for translation. Calculated differences for the talocrural joint were up to 4.7mm and  $12.1^\circ$  for translation and rotation respectively. Translation and rotation differences for the subtalar joint were up to 2.3mm and  $8.9^\circ$  respectively. Progressive changes in orientation and position of the axis of rotation were also shown.

**Conclusions:** This study demonstrated that kinematic changes due to ligament failure can be detected with 4DCT. It highlighted the possibility of adopting such method to investigate joint kinematics when pathological conditions are present.

**Keywords:** **Dynamic CT; Musculoskeletal Imaging; Ankle Ligaments; Joint Kinematics**

## 1. Introduction

Four-dimensional computed tomography (4DCT) is an upcoming imaging modality, initially due to the specific demand in cardiac and respiratory imaging and oncological applications [1–4]. The last decade, the validity, reliability and applicability of 4DCT for musculoskeletal (MSK) investigations have been explored [5–7]. Within this modality, three main applications have been reported so far: the evaluation of neurovascular entrapment, bony impingement and snapping, the estimation of sufficiency of intra-articular ligaments and the analysis of complex motion in several joints with strong rotatory components [8]. Hitherto, most MSK-studies using 4DCT have focused on the wrist joint. During a dart-throwing motion, 4DCT can detect differences in motion between the scaphoid and lunate in patients with scapholunate ligament disruption [9]. In patients with wrist pain, suspicious for scapholunate ligamentous injury, 4DCT could detect an increase in scapholunate interval, where plain radiographs were inconclusive [10]. In addition, 4DCT was able to detect various carpal abnormalities such as a trigger lunate, where plain radiographs, ultrasound and magnetic resonance imaging failed. Vacuum phenomena, subluxations and instabilities of the capitate and pisiform bones in patients with midcarpal instability were also demonstrated [11–15]. For the patellofemoral joint, 4DCT could visualise and quantify patella maltracking and patellofemoral instability [16–19]. As such, grade 2 and 3 J-sign maltracking with >2 quadrants lateralization of the patella in extension were predictive for symptomatic patellar instability [20]. In patients with femoroacetabular impingement and snapping scapula syndrome, 4DCT showed its usefulness in preoperative planning [21, 22]. 4DCT also showed its capability to evaluate joint kinematics during clinical tests. During the Bell-van Riet-test in asymptomatic acromioclavicular joints it was shown that the main movement of the clavicle was a posterior and superior translation [23]. In a case report on a malunion of a distal humeral metaphyseal fracture with a spurlike bone density overlying the anteromedial aspect of the distal humerus, 4DCT was used to evaluate movement restriction in the elbow. Imaging findings were confirmed during surgery [24]. Studies attempting to simulate pathological conditions showed that 4DCT may be able to detect altered joint kinematics. Simulation of subtalar joint instability, by means of subsequent sectioning of the cervical ligament and the interosseous talocalcaneal ligament, showed increases in joint amplitude [25]. In a similar study where the scapholunate ligaments were cut to mimic scapholunate instability, orthopaedic surgeons could discern images before and after induced ligamentous damage. After ligament section, the movement of the scaphoid increased up to 1.39mm compared to its original

position. These findings support the added value of 4DCT for diagnosing carpal instabilities associated with ligamentous damage where static imaging techniques fail [26, 27].

4DCT was shown to be reliable for musculoskeletal application, as errors below 1° and 1mm regarding rotation and translation values have been reported [28, 29]. Moreover, a wrist study showed strong inter-observer reliability for anteroposterior interval difference measurements in the pisotriquetral joint [30].

Consequently, there is a body of evidence supporting that 4DCT may be of value in musculoskeletal diagnosis and evaluation of musculoskeletal interventions. However, the capability and reproducibility of 4DCT to detect small differences in motion is still under investigation. So far, no studies concerning 4DCT analysing the talocrural joint (patho)kinematics have been reported. Therefore, the objective of this study was to explore the capacity of 4DCT to detect kinematic changes during full motion sequence of the talocrural and subtalar joint, provoked by sequential sectioning of the lateral collateral ligaments of the ankle.

## **2. Materials and Methods**

### ***2.1. Specimen***

One fresh frozen right leg was used for this study. To preserve the attachments of the tendons, the specimen's lower limb was cut above the distal third of the thigh. Four different scenarios were investigated. Initially, the movement with the lateral compartment of the ankle intact was studied (Scenario 1). Subsequently, the movements after consecutive sectioning of the anterior talo-fibular ligament (ATFL) (Scenario 2), the calcaneo-fibular ligament (CFL) (Scenario 3) and the posterior talo-fibular ligament (PTFL) (Scenario 4) were investigated. Approval from the medical ethical review board from the university hospital UZ Brussels was obtained before the start of this study (B.U.N 143201630099).

### ***2.2. Experimental setup***

A wide beam CT (256-slice, GE Revolution Healthcare) was used for dynamic acquisition in this study with the following parameters: 80kVp, 25mA, 0.28s gantry rotation time, 120mm z-axis coverage and 1.25mm slice thickness. Each scan had a continuous acquisition time of 3.92s and an estimated effective dose of 0.005mSv (1.9mGy CTDIvol).

A custom-made wooden device (Figure 1) was used to manually induce movement of the ankle at a pace of 25 cycles per minute. The device simulated the ankle movement from maximum dorsiflexion to full inversion and back. To prevent unwanted movement during acquisition two pins through the tibia fixed the specimen onto the device and the device was secured onto the CT table. A system of pulleys and a cable guided the movement. Four repetitions were performed to check repeatability and consistency of the motion prior to ligament sectioning.

Four dynamic acquisitions were performed for each scenario to obtain a total of 16 dynamic data sets.

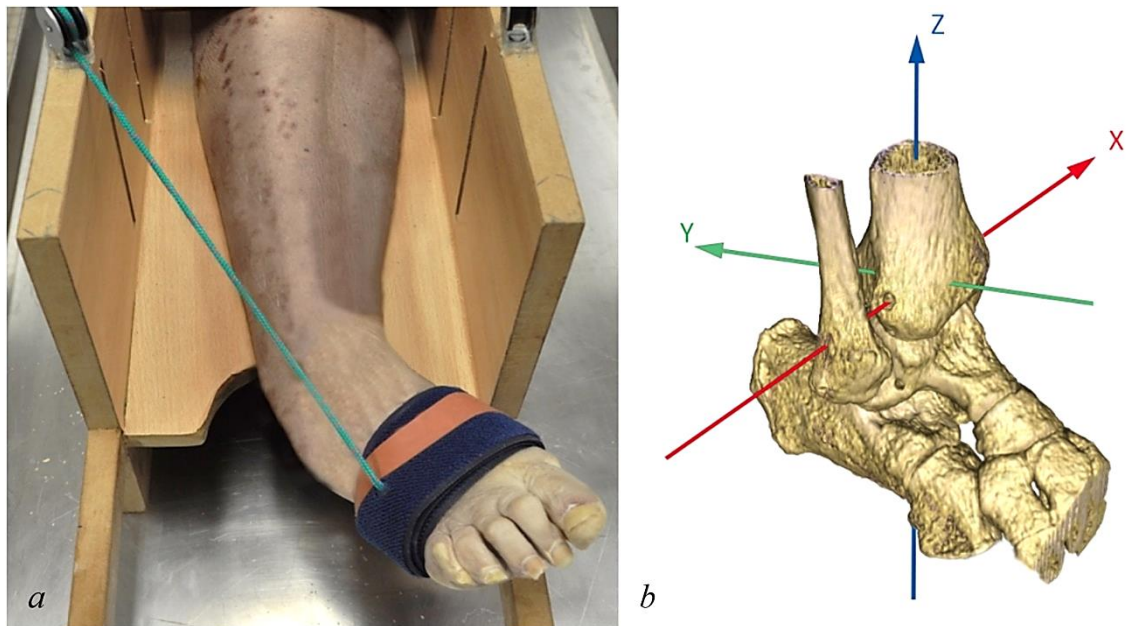


**Figure 1: Setup and reference frame.**

Experimental setup (a); Reference frame (b). X: dorsiflexion-plantarflexion/medio-lateral translation; Y: pronation-supination/anterior-posterior translation; Z: abduction-adduction/cranio-caudal translation.

### 2.3. Imaging processing

A total of 18 3D DICOM images, corresponding to phases of the motion from maximum dorsiflexion to full inversion, were processed to form a 4D image dataset (dynamic 3D volume dataset of the motion). The processing was performed according to a fixed workflow (Figure 2) using a C++ code based on the Insight Segmentation and Registration Toolkit (ITK) [31]. The calcaneus, talus and tibia were semi-automatically segmented from the volume image depicting the ankle at maximum dorsiflexion (the reference image). The segmented bones served as masks for the registration process which can be described as an optimization problem over the parameters  $\mu$  of the spatial transformation  $T_{\mu}$ .

$$\hat{\mu} = \arg \min_{\mu} \mathcal{C} \left( f(x), g \left( \left( \mathcal{T}_{\mu}(x) \right) \right) \right) \quad (1)$$

The registration is guided by minimizing a cost function  $\mathcal{C}$  (similarity metric) where  $f$  and  $g$  represent the fixed and moving images respectively and  $x$  represents the spatial coordinates over the image domains.

Using mutual information as the similarity metric, the three bones in the remaining dynamic sequence (moving images) were rigidly registered to their corresponding bones in the reference image dataset. The rigid registration was performed using Elastix, an open source software (<http://elastix.isi.uu.nl/>), based on ITK [32, 33]. The registration process resulted in 17 transformation matrices which aligned each of the moving images to the reference image.

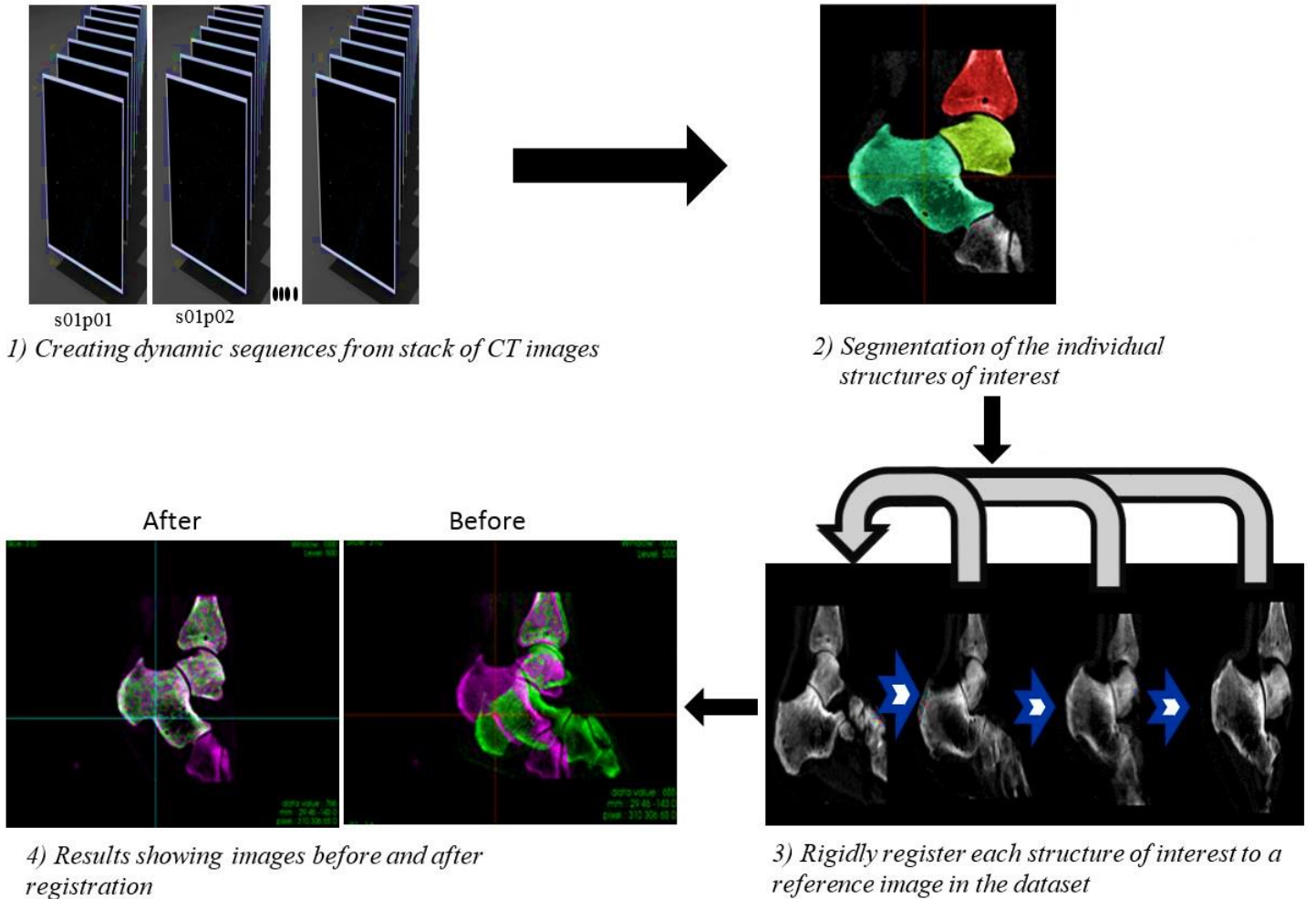


**Figure 2: Workflow of the image processing.**

#### ***2.4. Kinematic analysis***

The longitudinal axis of the tibia was aligned with the Z-axis of the CT. The X-axis, perpendicular to the Z-axis, passed through the medial malleolus and the medial malleolus was positioned at a height of zero along the Y-axis. This procedure and the fact that the CT was zeroed in that position before acquisition, allowed to use the technical reference frame of the device for kinematic calculation of the talus and calcaneus. The orientation of the reference frame is shown in Figure 1b. The positioning was guided by the scanner's on-board lasers.

Transformation matrices obtained from the registration were used to calculate three different kinematic parameters to describe talocrural and subtalar joint motion:

- a) translation of the center of the trochlea tali and the centroid of the calcaneus;
- b) rotation angles of the talus relative to the tibia and of the calcaneus relative to the talus;
- c) the study of the axis of rotation of the talocrural joint expressed as the finite helical axis (FHA).

The angles were calculated based on Cardan conventions. ZYX and ZXY angle composition sequences were adopted for the talocrural joint and the subtalar joint respectively.

#### ***2.5. Data analysis***

Differences between the four repetitions of Scenario 1 were explored to investigate repeatability of the setup. Differences between Scenario 1 and the other scenarios were reported using maximum differences and graphical representations. Changes of the axis of rotation were reported using orientation and position of the axis. The axes were visualized through combined 2D graphical representations.

### 3. Results

Four acquisitions were collected for each scenario. However, only one acquisition for Scenario 3 was available because of data transfer failure from the CT server to the archive.

#### 3.1. Repeatability

Between the four repetitions, the maximum differences for the talocrural joint rotational components were  $0.81^\circ$ ,  $0.37^\circ$  and  $0.89^\circ$  around the X-, Y- and Z-axis respectively. For the translations, these maximum differences were 0.27mm, 0.66mm and 0.08mm respectively. Maximum differences for the subtalar joint rotation angles and translations were  $1.01^\circ$ ,  $0.16^\circ$  and  $0.16^\circ$  and 0.24mm, 0.15mm and 0.64mm for the X-, Y- and Z-axis respectively. The axis of rotation, defined by the FHA, presented a consistent orientation during the four repetitions for both the talocrural and subtalar joint (Table 1 and Figure 3).

*Table 1: Rotation angles, translations and axis of rotation for Scenario 1 (intact).*

Rotation angles talocrural joint (deg $^\circ$ )				Rotation angles subtalar joint (deg $^\circ$ )		
Rep	X	Y	Z	X	Y	Z
1	37.81	-1.97	12.36	5.49	-16.66	-0.99
2	37.81	-1.80	12.18	5.64	-16.57	-0.90
3	37.78	-1.88	12.19	5.71	-16.65	-0.91
4	37.00	-1.60	11.47	6.50	-16.73	-1.06
Translations talocrural joint (mm)				Translations subtalar joint (mm)		
Rep	X	Y	Z	X	Y	Z
1	0.10	-11.08	-5.94	3.16	0.33	-2.25
2	-0.14	-11.28	-5.92	3.17	0.36	-2.15
3	-0.06	-11.22	-5.86	3.12	0.32	-2.07
4	-0.17	-10.62	-5.87	3.36	0.47	-1.61
Axis of rotation talocrural joint				Axis of rotation subtalar joint		
Rep	Translation (mm)	Rotation (deg $^\circ$ )	Vector X / Y / Z	Translation (mm)	Rotation (deg $^\circ$ )	Vector X / Y / Z
1	0.40	43.23	-0.77 / 0.15 / -0.23	0.39	17.46	-0.16 / 0.51 / 0.00
2	0.39	43.40	-0.77 / 0.15 / -0.23	0.40	17.61	-0.16 / 0.51 / 0.01
3	0.44	43.62	-0.77 / 0.15 / -0.23	0.40	17.63	-0.16 / 0.51 / 0.01
4	0.38	43.53	-0.77 / 0.15 / -0.23	0.41	17.74	-0.16 / 0.51 / 0.01

*Rep: repetition; Vector: orientation vector describing the orientation of the axis; deg $^\circ$ : degrees; mm: millimeter.*

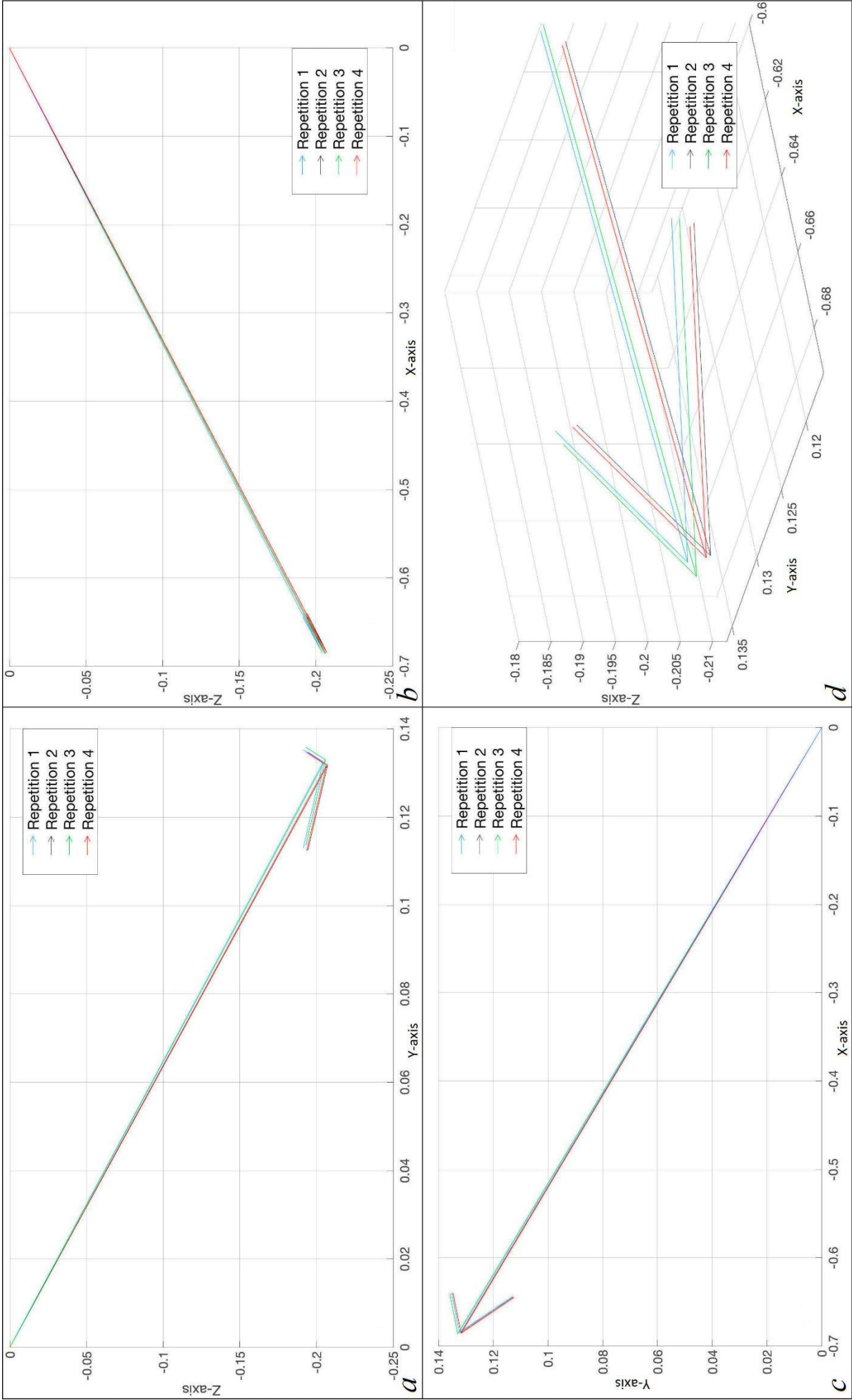


**Figure 3: Axis of rotation orientation for Scenario 1 (intact) for the talocrural joint.** Orientation on the YZ plane (a); Orientation on the XZ plane (b); Orientation on the XY plane (c); Enlargement showing the four different axes of rotation (d).

### 3.2. Differences between scenarios

For the talocrural joint, differences over the complete motion detected for rotation around the X-, Y- and Z-axis between Scenario 1 (intact) and Scenario 2 (section of ATFL) ranged from 5.28° to 6.77°. For the subtalar joint, these differences varied between 0.62° and 2.67°. Values concerning the translations along the axes varied from 0.68mm to 3.02mm for the talocrural joint and from 0.35mm to 1.33mm for the subtalar joint.

Comparing motion between Scenario 1 and Scenario 3 (section of ATFL and CFL), rotation angle differences varied from 6.48° to 9.27° for the talocrural joint. For the subtalar joint these values varied from 1.33° to 4.37°. The translations for this comparison varied between 1.25mm and 3.78mm for the talocrural joint. Regarding the subtalar joint, there was a variation between 0.29mm and 1.38mm.

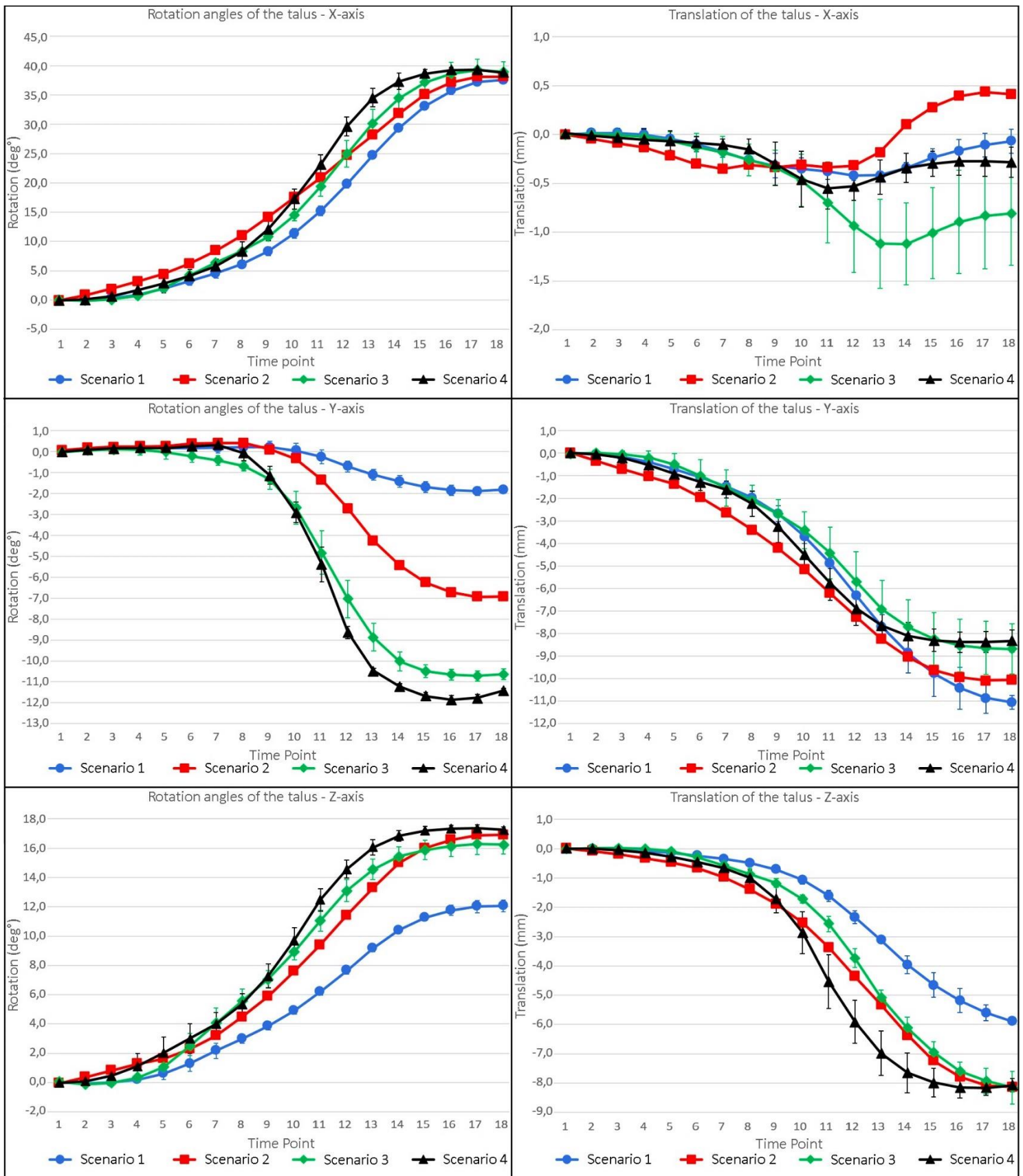
The comparison of motion between Scenario 1 and Scenario 4 (section of the ATFL, CFL and PTFL), showed rotation angle differences varying from 7.80° to 12.14° for the talocrural joint. For the subtalar joint values varied from 2.37° to 8.88°. Translation differences ranged between 0.49mm and 4.73mm for the talocrural joint and between 0.52mm and 2.30mm for the subtalar joint.

Table 2 summarizes the maximum differences and a graphical representation of the rotation and translation values at the level of the talocrural and subtalar joint at the different time points of the movement is provided in Figure 4 and Figure 5.

**Table 2: Absolute maximum differences between scenarios over the course of the movement.**

Rotation angles talocrural joint			
	X (MAX)	Y (MAX)	Z (MAX)
	(deg°)	(deg°)	(deg°)
Scenario 1 VS Scenario 2	6.77	5.28	5.28
Scenario 1 VS Scenario 3	8.27	9.27	6.48
Scenario 1 VS Scenario 4	12.14	10.48	7.80
Rotation angles subtalar joint			
	X (MAX)	Y (MAX)	Z (MAX)
	(deg°)	(deg°)	(deg°)
Scenario 1 VS Scenario 2	0.62	2.67	1.48
Scenario 1 VS Scenario 3	1.33	4.37	2.23
Scenario 1 VS Scenario 4	4.53	8.88	2.37
Translations talocrural joint			
	X (MAX)	Y (MAX)	Z (MAX)
	(mm)	(mm)	(mm)
Scenario 1 VS Scenario 2	0.68	1.89	3.02
Scenario 1 VS Scenario 3	1.25	3.78	3.11
Scenario 1 VS Scenario 4	0.49	3.51	4.73
Translations subtalar joint			
	X (MAX)	Y (MAX)	Z (MAX)
	(mm)	(mm)	(mm)
Scenario 1 VS Scenario 2	1.27	0.35	1.33
Scenario 1 VS Scenario 3	0.85	0.29	1.38
Scenario 1 VS Scenario 4	2.30	0.52	1.69

*X: dorsiflexion-plantarflexion/medio-lateral; Y: pronation-supination/anterior-posterior; Z: abduction-adduction/cranio-caudal; MAX: maximum difference; deg°: degrees; mm: millimeter; Scenario 1: intact; Scenario 2: section of ATFL; Scenario 3: section of ATFL and CFL; Scenario 4: section of ATFL, CFL and PTFL.*



**Figure 4: Rotation angles and translations of the scenarios for the talocrural joint over the course of the movement.** Each curve represents the mean of four repetitions. Scenario 1: intact; Scenario 2: section of ATFL; Scenario 3: section of ATFL and CFL; Scenario 4: section of ATFL, CFL and PTFL.

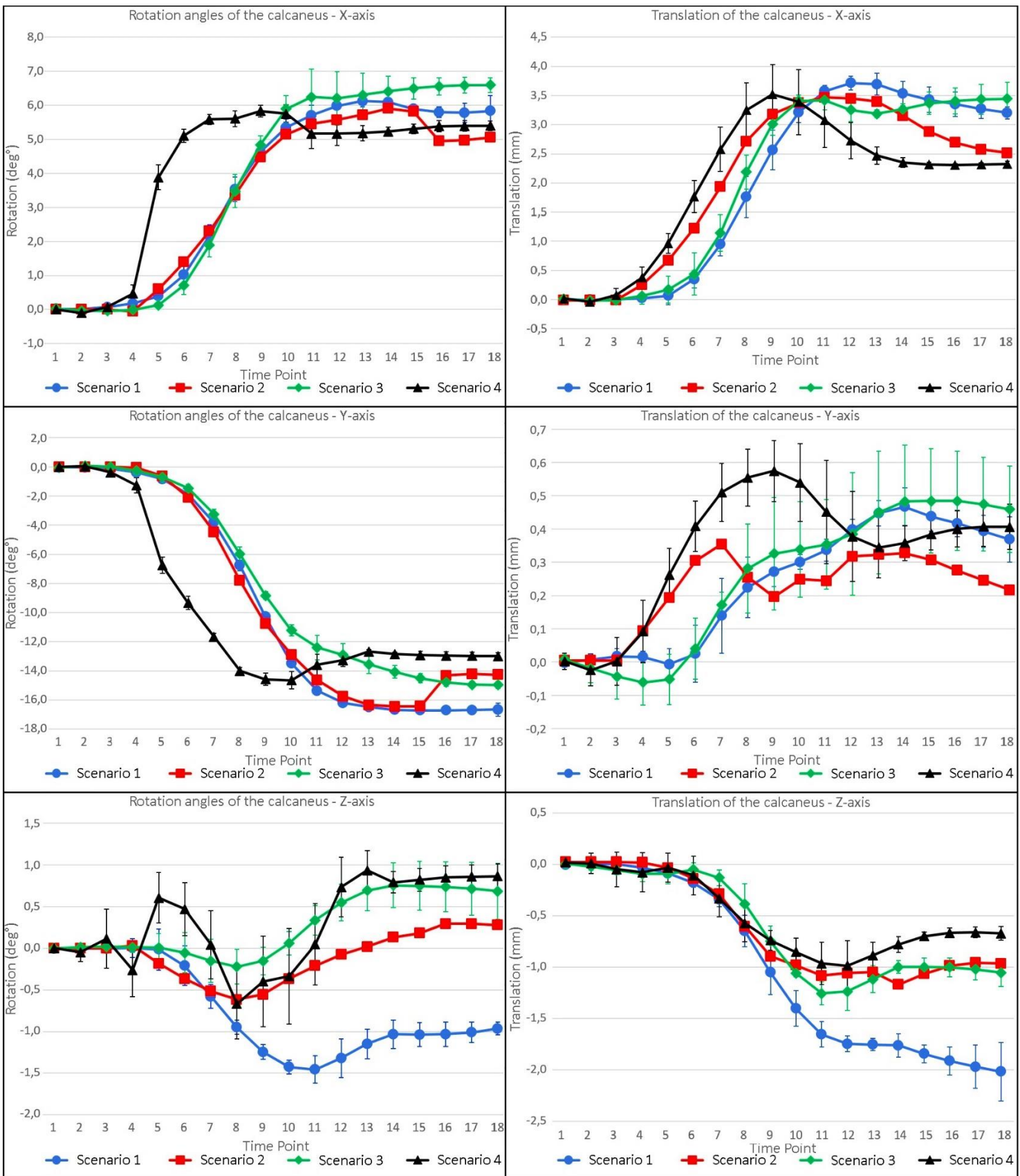


**Figure 5: Rotation angles and translations of the scenarios for the subtalar joint over the course of the movement.** Each curve represents the mean of four repetitions. Scenario 1: intact; Scenario 2: section of ATFL; Scenario 3: section of ATFL and CFL; Scenario 4: section of ATFL, CFL and PTFL.

The axis of rotation had a maximum change in orientation between the intact scenario and the others of  $-20.6^\circ$  ( $\alpha$  angle Figure 6a) on the YZ plane,  $13.7^\circ$  ( $\beta$  angle Figure 6b) on the XY plane and  $4.1^\circ$  ( $\gamma$  angle Figure 6c) on the XZ plane. A progressive translation of the axis up to 4.13mm in postero-cranial direction was observed (Figure 6d). Table 3 shows the single components of each axis for orientation and plane intersection.

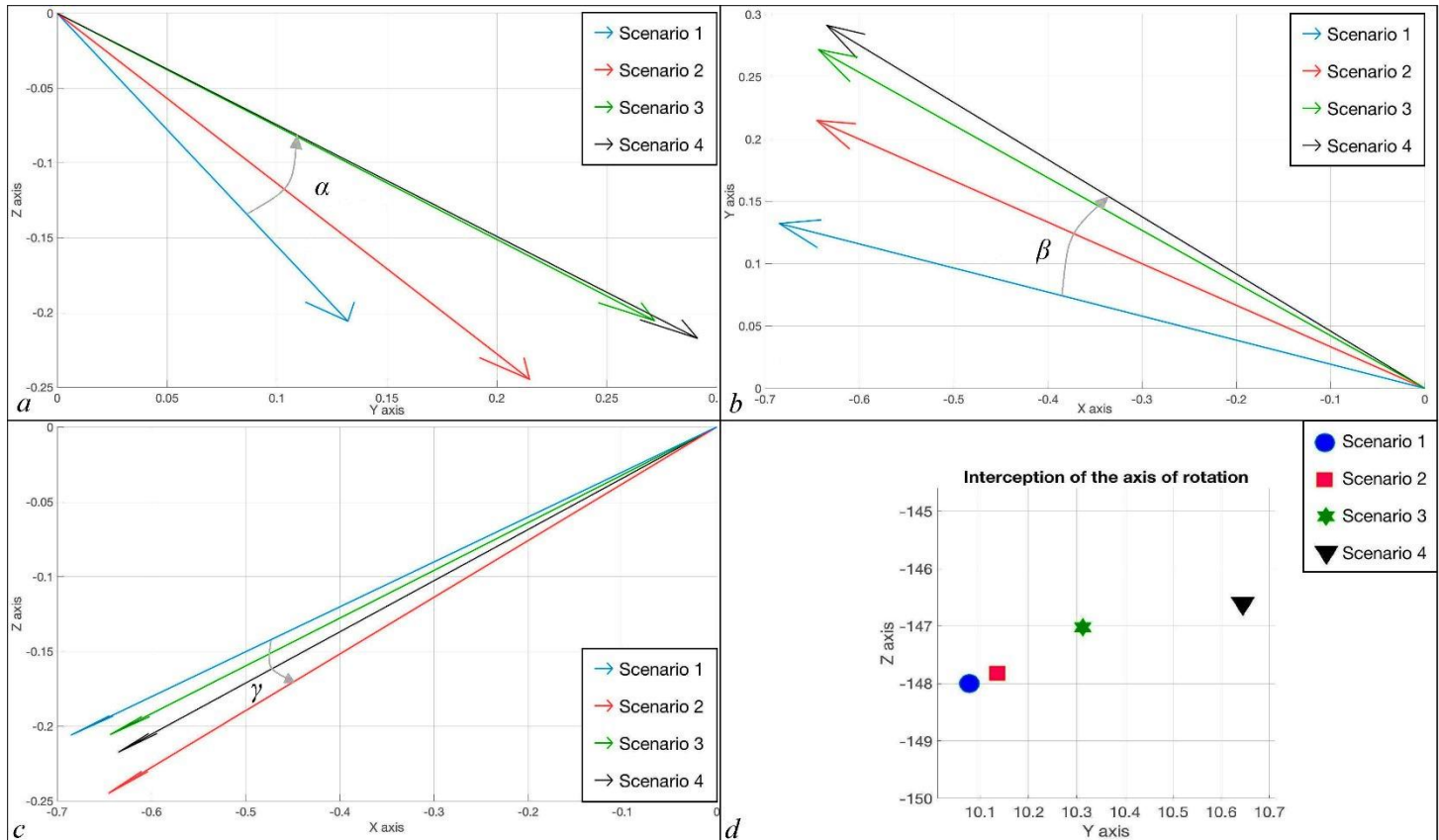


**Figure 6: Changes in the axis of rotation for the different scenarios.**

Each scenario is the average of 4 repetitions. Changes in orientation of the axis of rotation for the YZ (a), XY (b) and XZ (c) plane; Differences in the interception with the YZ plane passing through the center of the articular surface of the talus (d). FHA: finite helical axis; Scenario 1: intact; Scenario 2: section of ATFL; Scenario 3: section of ATFL and CFL; Scenario 4: section of ATFL, CFL and PTFL;  $\alpha$  angle: Scenario 1 vs Scenario 4;  $\beta$  angle: Scenario 1 vs Scenario 2;  $\gamma$  angle: Scenario 1 vs Scenario 4.

**Table 3: Orientation of the axis of rotation.**

Axis of rotation talocrural joint						
	Orientation X-component	Orientation Y-component	Orientation Z-component	Interception X-axis	Interception Y-axis	Interception Z-axis
Scenario 1	-0,77	0,15	-0,23	11,46	10,08	-148,00
Scenario 2	-0,72	0,24	-0,28	11,46	10,46	-147,08
Scenario 3	-0,72	0,31	-0,23	11,46	11,58	-144,87
Scenario 4	-0,71	0,33	-0,24	11,46	11,62	-144,16

Orientation X, Y and Z: orientation vector components describing the orientation of the axis; Interception X, Y and Z: interception of the axis of rotation with a plane parallel to the YZ plane, passing through the centre of the talus; Scenario 1: intact; Scenario 2: section of ATFL; Scenario 3: section of ATFL and CFL; Scenario 4: section of ATFL, CFL and PTFL.

## 4. Discussion

The objective of this study was to explore the possibility of 4DCT to detect kinematic changes in the talocrural and subtalar joint induced by sequential sectioning of the lateral collateral ligaments of the ankle. Lateral collateral ligament sprains are the most commonly reported injury diagnoses [34]. Therefore, the kinematic changes associated with such injury are of great importance from a clinical perspective.

The current study showed that 4DCT may be applicable for evaluating joint kinematics in various situations. Rotation angle differences between repetitions around the X-, Y- and Z-axis were below  $1^\circ$  and below 1mm for translation values for the talocrural joint. Such small differences together with a consistent orientation of the axis of rotation, highlight the repeatability of the setup used in this study.

Similar to dual-fluoroscopy and dynamic magnetic resonance imaging, 4DCT has the capability to detect changes which occur merely during movement. This makes it possible to compare not only the start and end positions, but each time point of the motion. Moreover, the high temporal and spatial resolution of 4DCT, its availability and the lower costs compared to MRI, makes it a good candidate to explore in vivo joint kinematics in high detail without the limitations related to other motion acquisition devices.

In the current study, looking only at the beginning and end of the movement, it would not always have been possible to clearly distinguish the four scenarios. On the contrary, an analysis of differences in movement during the motion showed clear changes between the intact ankle and after ligament section.

Concerning the rotation angles for the talocrural joint a progressive increase in maximum difference around all three axes was seen with every cut. The biggest difference was found around the X-axis. A similar trend was observed for the subtalar joint. However, the biggest difference here was observed around the Y-axis. Looking at the translation values for the talocrural and subtalar joint, no such trend as seen for the rotation values was found.

In a more clinical perspective, there was no real increase in plantarflexion range of motion in the talocrural joint after ligament section, but only a different motion pattern. On the other hand, there was an increase in supination and adduction combined with a different motion pattern. For the subtalar joint there weren't big differences in range of motion between scenarios concerning plantarflexion. However, a big difference was seen in motion pattern for Scenario 4. Overall a little less supination was seen with ligament section, but again a much different motion pattern was observed for Scenario 4. The switch from abduction to adduction after ligament section was the most notable

difference for the subtalar joint. Also, a jerkier motion pattern was observed for Scenario 4 to obtain this adduction.

Regarding the translations, decreased anterior translation and different motion patterns with every cut were observed for the talocrural joint. Overall there was a constant increased caudal translation for every ligament section, but with different motion patterns. Greatest variability was found for the medio-lateral translation. Where Scenario 1 and 4 almost showed the same pattern and end position (small lateral translation), Scenario 2 showed an increased lateral translation and Scenario 3 a medial translation. For the subtalar joint no big differences in medio-lateral and antero-posterior translation were seen concerning the end position. However, Scenario 2 and 4 showed much different motion patterns along the Y-axis compared to Scenario 1. Last, a decreased caudal translation was seen for Scenario 2 through 4 in the subtalar joint. These kinematic modifications, based on Cardan angles and translations, caused a different orientation and position of the axis of rotation for both the talus and the calcaneus after ligament sectioning.

In a similar study, Teixeira et al. (2017) tried to reproduce joint instability in the subtalar joint by cutting the cervical ligament of the ankle and the interosseous talo-calcaneal ligament. It was found that 4DCT was able to detect small changes in joint amplitude.

These preliminary findings may support the evidence that 4DCT is of added value in evaluating joint pathologies such as instabilities associated with ligamentous damage. Moreover, based on the findings of the current study it seems feasible to detect small changes during dynamic acquisition. These findings are in line with earlier studies on the wrist and thumb joint where 4DCT showed to be able to detect differences below  $1^\circ$  and 1mm [28, 29].

Besides kinematic analysis, radiation dose has also to be considered, because the potential risk of radiation exposure is a drawback for computed tomography. A commonly used metric to track radiation dose in patients is the effective dose measured in millisieverts. This metric takes the absorbed dose, received by the irradiated organs in the scan region, and the radiation sensitivity of the organs into account [35]. In general, exposure to peripheral joints result in a lower effective dose compared to body regions closer to the trunk due to the absence of important radiosensitive tissues [36]. Earlier studies on the wrist and hand showed doses ranging between 0.02mSv and 1.43mSv [6, 7, 9–14, 26–30, 37–42]. Similar values were found for the knee (0.1mSv - 1.57mSv) and elbow (0.51mSv) [16–20, 24, 43]. Teixeira et al. (2017) also reported doses of 0.01mSv in a study on the subtalar joint. The current study showed an effective dose of 0.005mSv

(1.9mGy CTDI<sub>vol</sub>). Considering the fact that the yearly background radiation varies from 2mSv – 3mSv, these values are acceptable for using 4DCT in vivo [28, 29, 44–46].

The current study had some limitations. First, kinematics of an in vitro setup may not exactly reflect normal physiological movements of a living subject. However, the movement was externally controlled in this study to increase the reproducibility and to avoid a high radiation dose in a living subject due to the high number of repetitions. Secondly, only one specimen was available for this study, limiting the statistical analysis. Third, the movement was manually induced, making the setup susceptible to errors due to differences in applied loads. However, comparison of repetitions showed that the setup was reliable with differences smaller than 1mm and 1° between repetitions. Moreover, variability of the four repetitions for each scenario was taken into account when maximum values were calculated. Last, the skin dose was not measured in this study. Dynamic CT acquisition is based on scanning the same area over a period of time and even in the presence of a high skin dose, the effective dose can remain low. Thus, although our study reported very low CTDI<sub>vol</sub> showing a low radiation exposure, the skin dose may be a more sensitive parameter to determine radiation exposure and should be measured in further clinical studies.

## 5. Conclusion

This study demonstrated that kinematic changes in the talocrural and subtalar joint, due to lateral collateral ankle ligament failure, can be detected with 4DCT. Sequential sectioning of the lateral collateral ankle ligaments progressively increased the angular motion and changed the amount and direction of bony translation in both joints. The change in orientation of the axis of rotation was also highlighted. It was also shown that more ligamentous damage induced more changes in kinematics compared with an intact scenario. Due to the high temporal and spatial resolution of 4DCT, detailed acquisition of in vivo situations is possible. As such, this method can be used to investigate pathologies that present themselves predominantly during motion. Quantifying the amount of lateral collateral ankle ligament damage could help the clinician to choose the optimal treatment. 4DCT seems capable of obtaining this with a very small radiation exposure for the patient. Further studies with bigger in vivo sample sizes are recommended to confirm the current findings and offer reference values suitable for clinical practice.

## References

1. Hamdan A, Guetta V, Konen E, et al (2012) Deformation dynamics and mechanical properties of the aortic annulus by 4-dimensional computed tomography: Insights into the functional anatomy of the aortic valve complex and implications for transcatheter aortic valve therapy. *J Am Coll Cardiol* 59:119–127 . doi: 10.1016/j.jacc.2011.09.045
2. Schievano S, Capelli C, Young C, et al (2011) Four-dimensional computed tomography: A method of assessing right ventricular outflow tract and pulmonary artery deformations throughout the cardiac cycle. *Eur Radiol* 21:36–45 . doi: 10.1007/s00330-010-1913-5
3. Beland MD, Monchik JM (2012) 4d ct – a diagnostic tool to localize an occult Parathyroid adenoma in a Patient With Primary Hyperparathyroidism. *Med Heal R I* 1–2
4. Tan K V., Thomas R, Hardcastle N, et al (2015) Predictors of respiratory-induced lung tumour motion measured on four-dimensional computed tomography. *Clin Oncol* 27:197–204 . doi: 10.1016/j.clon.2014.12.001
5. Gondim Teixeira PA, Formery AS, Hossu G, et al (2017) Evidence-based recommendations for musculoskeletal kinematic 4D-CT studies using wide area-detector scanners: a phantom study with cadaveric correlation. *Eur Radiol* 27:437–446 . doi: 10.1007/s00330-016-4362-y
6. Kerkhof FD, Brugman E, D’Agostino P, et al (2016) Quantifying thumb opposition kinematics using dynamic computed tomography. *J Biomech* 49:1994–1999 . doi: 10.1016/j.jbiomech.2016.05.008
7. Tay SC, Primak AN, Fletcher JG, et al (2007) Four-dimensional computed tomographic imaging in the wrist: Proof of feasibility in a cadaveric model. *Skeletal Radiol* 36:1163–1169 . doi: 10.1007/s00256-007-0374-7
8. Teixeira PAG, Gervaise A, Louis M, et al (2015) Musculoskeletal Wide-Detector CT Kinematic Evaluation: From Motion to Image. *Semin Musculoskelet Radiol* 19:456–462 . doi: 10.1055/s-0035-1569257
9. Garcia-Elias M, Alomar Serrallach X, Monill Serra J (2014) Dart-throwing motion in patients with scapholunate instability: a dynamic four-dimensional computed tomography study. *J Hand Surg (European Vol)* 39:346–352 . doi: 10.1177/1753193413484630

10. Demehri S, Hafezi-Nejad N, Morelli JN, et al (2016) Scapholunate kinematics of asymptomatic wrists in comparison with symptomatic contralateral wrists using four-dimensional CT examinations: initial clinical experience. *Skeletal Radiol* 45:437–446 . doi: 10.1007/s00256-015-2308-0
11. Repse SE, Koulouris G, Troupis JM (2015) Wide field of view computed tomography and mid carpal instability: The value of the sagittal radius-lunate-capitate axis - Preliminary experience. *Eur J Radiol* 84:908–914 . doi: 10.1016/j.ejrad.2015.01.020
12. Repse SE, Amis B, Troupis JM (2014) Four-dimensional computed tomography and detection of dynamic capitate subluxation. *J Med Imaging Radiat Oncol* 59:1–5 . doi: 10.1111/1754-9485.12260
13. Demehri S, Wadhwa V, Thawait GK, et al (2014) Dynamic Evaluation of Pisotriquetral Instability Using 4-dimensional Computed Tomography. *J Comput Assist Tomogr* 38:507–512 . doi: 10.1097/RCT.0000000000000074
14. Halpenny D, Courtney K, Torreggiani WC (2012) Dynamic four-dimensional 320 section CT and carpal bone injury - A description of a novel technique to diagnose scapholunate instability. *Clin Radiol* 67:185–187 . doi: 10.1016/j.crad.2011.10.002
15. Troupis JM, Amis B (2013) Four-dimensional computed tomography and trigger lunate syndrome. *J Comput Assist Tomogr* 37:639–43 . doi: 10.1097/RCT.0b013e31828b68ec
16. Tanaka MJ, Elias JJ, Williams AA, et al (2016) Characterization of patellar maltracking using dynamic kinematic CT imaging in patients with patellar instability. *Knee Surgery, Sport Traumatol Arthrosc* 24:3634–3641 . doi: 10.1007/s00167-016-4216-9
17. Tanaka MJ, Elias JJ, Williams AA, et al (2015) Correlation Between Changes in Tibial Tuberosity-Trochlear Groove Distance and Patellar Position During Active Knee Extension on Dynamic Kinematic Computed Tomographic Imaging. *Arthroscopy* 31:1748–1755 . doi: 10.1016/j.arthro.2015.03.015
18. Williams AA, Elias JJ, Tanaka MJ, et al (2016) The Relationship Between Tibial Tuberosity-Trochlear Groove Distance and Abnormal Patellar Tracking in Patients With Unilateral Patellar Instability. *Arthroscopy* 32:55–61 . doi: 10.1016/j.arthro.2015.06.037

19. Demehri S, Thawait GK, Williams AA, et al (2014) Imaging characteristics of contralateral asymptomatic patellofemoral joints in patients with unilateral instability. *Radiology* 273:821–30 . doi: 10.1148/radiol.14140295
20. Tanaka MJ, Williams A, Elias JJ, et al (2015) Characterizing Patterns In Patellar Maltracking On Dynamic Kinematic CT Imaging. *Orthop J Sport Med* 3:2015 . doi: 10.1177/2325967115S00014
21. Wassilew GI, Janz V, Heller MO, et al (2013) Real time visualization of femoroacetabular impingement and subluxation using 320-slice computed tomography. *J Orthop Res* 31:275–281 . doi: 10.1002/jor.22224
22. Bell SN, Troupis JM, Miller D, et al (2015) Four-dimensional computed tomography scans facilitate preoperative planning in snapping scapula syndrome. *J Shoulder Elb Surg* 24:e83–e90 . doi: 10.1016/j.jse.2014.09.020
23. Alta TD, Bell SN, Troupis JM, et al (2012) The new 4-dimensional computed tomographic scanner allows dynamic visualization and measurement of normal acromioclavicular joint motion in an unloaded and loaded condition. *J Comput Assist Tomogr* 36:749–54 . doi: 10.1097/RCT.0b013e31826dbc50
24. Goh YP, Lau KK (2012) Functional Assessment of the Elbow Joint. *Am J Orthop* 20–22
25. Teixeira PAG, Formery AS, Jacquot A, et al (2017) Quantitative analysis of subtalar joint motion with 4D CT: Proof of concept with cadaveric and healthy subject evaluation. *Am J Roentgenol* 208:150–158 . doi: 10.2214/AJR.16.16434
26. Mat Jais IS, Tay SC (2017) Kinematic analysis of the scaphoid using gated four-dimensional CT. *Clin Radiol* 72:794.e1-794.e9 . doi: 10.1016/j.crad.2017.04.005
27. Leng S, Zhao K, Qu M, et al (2011) Dynamic CT technique for assessment of wrist joint instabilities. *Med Phys* 38 Suppl 1:S50 . doi: 10.1118/1.3577759
28. Zhao K, Breighner R, Holmes D, et al (2015) A Technique for Quantifying Wrist Motion Using Four-Dimensional Computed Tomography: Approach and Validation. *J Biomech Eng* 137:074501 . doi: 10.1115/1.4030405
29. Goto A, Leng S, Sugamoto K, et al (2014) In vivo pilot study evaluating the thumb carpometacarpal joint during circumduction. In: *Clinical Orthopaedics and Related Research*. pp 1106–1113
30. Demehri S, Hafezi-Nejad N, Thakur U, et al (2015) Evaluation of pisotriquetral motion pattern using four-dimensional CT: Initial clinical experience in asymptomatic wrists. *Clin Radiol* 70:1362–1369 . doi: 10.1016/j.crad.2015.07.007

31. Yoo TS, Ackerman MJ, Lorenzen WE, et al (2002) Engineering and algorithm design for an image processing API: A technical report on ITK - The Insight Toolkit. In: *Studies in Health Technology and Informatics*. pp 586–592
32. Klein S, Staring M, Murphy K, et al (2010) Elastix: A toolbox for intensity-based medical image registration. *IEEE Trans Med Imaging* 29:196–205 . doi: 10.1109/TMI.2009.2035616
33. Shamonin DP, Bron EE, Lelieveldt BPF, et al (2014) Fast parallel image registration on CPU and GPU for diagnostic classification of Alzheimer’s disease. *Front Neuroinform* 7:50 . doi: 10.3389/fninf.2013.00050
34. Roos KG, Kerr ZY, Mauntel TC, et al (2017) The Epidemiology of Lateral Ligament Complex Ankle Sprains in National Collegiate Athletic Association Sports. *Am J Sports Med* 45:201–209 . doi: 10.1177/0363546516660980
35. Wrixon AD (2008) New ICRP recommendations. *J. Radiol. Prot.* 28:161–168
36. Saltybaeva N, Jafari ME, Hupfer M, Kalender W a (2014) Estimates of effective dose for CT scans of the lower extremities. *Radiology* 273:153–159 . doi: 10.1148/radiol.14132903
37. Edirisinghe Y, Troupis JM, Patel M, et al (2014) Dynamic motion analysis of dart throwers motion visualized through computerized tomography and calculation of the axis of rotation. *J Hand Surg (European Vol* 39:364–372 . doi: 10.1177/1753193413508709
38. Mat Jais IS, Liu X, An KN, Tay SC (2014) A method for carpal motion hysteresis quantification in 4-dimensional imaging of the wrist. *Med Eng Phys* 36:1699–1703 . doi: 10.1016/j.medengphy.2014.08.011
39. Shores JT, Demehri S, Chhabra A (2013) Kinematic “4 Dimensional” CT Imaging in the Assessment of Wrist Biomechanics Before and After Surgical Repair. *Eplasty* 13:e9
40. Choi YS, Lee YH, Kim S, et al (2013) Four-dimensional real-time cine images of wrist joint kinematics using dual source CT with minimal time increment scanning. *Yonsei Med J* 54:1026–1032 . doi: 10.3349/ymj.2013.54.4.1026
41. Troupis JM, Amis B (2013) Four-dimensional Computed Tomography and Trigger Lunate Syndrome. *J Comput Assist Tomogr* 37:639–643 . doi: 10.1097/RCT.0b013e31828b68ec

42. Tay SC, Primak AN, Fletcher JG, et al (2008) Understanding the Relationship Between Image Quality and Motion Velocity in Gated Computed Tomography:Preliminary Work for 4-Dimensional Musculoskeletal Imaging. *J Comput Assist Tomogr* 32:634–639 . doi: 10.1097/RCT.0b013e31815c5abc
43. Forsberg D, Lindblom M, Quick P, Gauffin H (2016) Quantitative analysis of the patellofemoral motion pattern using semi-automatic processing of 4D CT data. *Int J Comput Assist Radiol Surg* 11:1731–1741 . doi: 10.1007/s11548-016-1357-8
44. UNSCEAR. United Nations Scientific Committee on the Effects of Atomic Radiation (2000) Sources and Effects of Ionizing Radiation
45. Biswas D, Bible JE, Bohan M, et al (2009) Radiation exposure from musculoskeletal computerized tomographic scans. *J Bone Jt Surg - Ser A* 91:1882–1889 . doi: 10.2106/JBJS.H.01199
46. Thurston J (2010) NCRP Report No. 160: Ionizing Radiation Exposure of the Population of the United States. *Phys Med Biol* 55:6327 . doi: 10.1088/0952-4746/29/3/B01